Eur. Phys. J. D **32**, 277–283 (2005)
DOI: 10.1140/epjd/e2005-00003-3

THE EUROPEAN PHYSICAL JOURNAL D

Ion charge state distributions following K-shell ionization in atoms

A.M. El-Shemi[1,a] and Y.A. Lotfy[2]

[1] Applied Sciences Department, College of Technological Studies, P.O. Box 42325, Shuwaikh 70654, Kuwait
[2] El-Minia University, Faculty of Science, Physics Department, 61111 El-Minia, Egypt

Received 20 May 2004 / Received in final form 14 September 2004
Published online 18 January 2005 –

Abstract. Ion charge state distributions and the mean charge state following K-shell ionization in atoms are calculated. The Monte Carlo method is applied to calculate the vacancy cascades after K-shell vacancy creation. The radiative and non-radiative transitions are calculated for singly ionized atoms. The transition rates for multi-ionized atoms are obtained using a statistical scaling procedure based on the transition probabilities for singly ionized atoms. The electron shake-off process due to the change of atomic potential, which occurs from core hole production and de-excitation decays, is considered in the calculation. The present results agree well with the available experimental values.

PACS. 32. Atomic properties and interactions with photons – 32.80.-t Photon interactions with atoms – 32.80.Fb Photoionization of atoms and ions

1 Introduction

Inner-shell ionization processes were analyzed under different points of view. Thereby, basic investigations of atomic properties as well as investigations in connection with other disciplines as solid state physics, plasma-physics, and astrophysics were of interest. Our interest is focused on the atomic reorganization cascades following inner-shell vacancy production and the creation of multiply ionized atoms. The importance of this process is based on the fact that atomic reorganization cascades in ionized atoms with different ion charge states are taking place, e.g. as result of a primary inner-shell vacancy, ions with different charge states can be created.

Atomic reorganization starts by filling the initially inner-shell vacancy by a radiative transition (X-ray) or by a non-radiative transition (Auger and Coster-Kronig processes). New vacancies created during this atomic reorganization may in turn be filled by further radiative and non-radiative transitions until all vacancies reach the outermost occupied shells (energetically stable final states or metastable ones because of relevant selection rules). In the case of X-ray processes the vacancy moves to an outer shell under emission of characteristic X-rays, while for non-radiative transitions one electron from an outer shell fills up the inner-shell vacancy and another electron is ejected into the continuum. With the exception of the K and L shells in heavy atoms, the Auger processes are much more probable than X-ray emission. The production of inner-shell vacancy in an atom and the de-excitation decays through radiative and non-radiative transitions may result in a change of the atomic potential; this change leads to the emission of an additional electron in the continuum (electron shake-off processes). In each Auger process ejecting an electron into the continuum, a serie of such events called vacancy cascade take place, gives rise to a highly charged ion.

The charge state distributions of ions resulting from de-excitation decay of inner-shell vacancies were studied both experimentally and theoretically. The multiply charged ions following vacancy cascades in rare gas atoms were measured at some restricted energies of photons that could be obtained from the X-ray tubes, and the produced ions were analyzed with a magnetic spectrometer [1–6]. The charge state distribution of ions as a function of photon energies were measured by sweeping the photon energy across the ionization threshold [7–11]. The initial inner-shell vacancy was produced by synchrotron radiation and the ion yields are analyzed by using a time-of-flight mass spectrometer.

There are two major approaches to calculate the vacancy cascades and the multiply charged ions following inner-shell vacancy production in atoms. The first method is based on straightforward construction of the de-excitation decay trees for radiative and non-radiative transitions [1,12–16]. The second method is based on simulation of all possible radiative and non-radiative pathways to fill the inner-shell vacancies in atoms [17–21].

In the present work, the charge state distributions of ions and the average of all charged ions being produced

[a] e-mail: admohamed@yahoo.com

from de-excitation decay of vacancies after K-shell ionization in atoms are calculated using the Monte Carlo (MC) simulation technique. The Monte Carlo (MC) algorithms are applied to simulate all possible pathways of radiative and non-radiative transitions to fill the K-shell vacancy in these atoms. The radiative transitions of singly ionized atoms are calculated using multiconfiguration Dirac Fock (MCDF) wave functions from Grant et al. [22]. The non-radiative transitions are calculated by using Dirac Fock Slater approximation by computer code written by Lorenz and Hartmann [23]. The electron shake-off processes due to the change of the atomic potential after inner shell vacancy production and non-radiative transitions are calculated with a code given by El-Shemi [24]. The results of final charge state distributions and the average number of ejected electrons are compared with available theoretical and experimental data.

2 Method of calculation

The initial states of the radiative (X-ray) and non-radiative (Auger and Coster-Kronig) transitions are created by inner-shell ionization in atoms. The inner-shell vacancies could be transferred into the ground state via a cascade of successive radiative and non-radiative transitions. The cascade of electron emission caused by the creation of an inner-shell vacancy in atom yields multiply charged ions.

The K-shell vacancy in an ^{1}S ground state atom gives rise to a ^{2}S ionic state in the atom

$$[\mathrm{A}] + h\upsilon \rightarrow [\mathrm{A}^+]1s^{-1}\,{}^2\mathrm{S}_{1/2} + e_e. \tag{1}$$

Here the target atom A is ionized in a first step, for instance by photoionization $h\upsilon$, e_e is the primary emitted electron. In the second step, the radiative (X-ray) and non-radiative transitions take place. If the decay of the K-shell vacancy occurs through a radiative transition, then a K_α photon is emitted, transferring the vacancy to the $2p$ subshell:

$$[\mathrm{A}^+]1s^{-1}\,{}^2\mathrm{S}_{1/2} \rightarrow [\mathrm{A}^+]2p^{-1}\,{}^2\mathrm{P}_{3/2,1/2} + h\upsilon'. \tag{2}$$

If the $2p$ vacancy is filled via Auger process this results in two $3p$ vacancies:

$$[\mathrm{A}^+]2p^{-1}\,{}^2\mathrm{P}_{1/2,3/2} \rightarrow [\mathrm{A}^{++}]3p^{-2}\,{}^1\mathrm{S}_0, {}^1\mathrm{D}_2, {}^3\mathrm{P}_{2,1,0} + e_{\mathrm{Auger}} \tag{3}$$

where A^+ is the resonant intermediate state and is usually referred to as the initial state of the transition. A^{++} is doubly ionized atom.

The calculation of final charge state distributions and the average number of ejected electrons following de-excitation decay of inner-shell vacancies have been carried out by Monte Carlo algorithms. This method is based on the simulation of all possible radiative and non-radiative pathways to fill the inner-shell vacancies in the atom. The calculation technique is used for simulating de-excitation cascade decays following inner-shell vacancy creation, considering fluorescence yields (radiative branching ratios), Auger and Coster-Kronig yields (non-radiative branching ratios), and electron shake-off processes. The radiative and non-radiative branching ratios are defined as the probability that the vacancy in an atom is filled through X-ray transitions (photon emission) or through Auger and Coster-Kronig processes, respectively. They are calculated as follows:

$$\text{fluorescence yield}\quad \omega(f \rightarrow i) = \frac{\Gamma_{if}^R}{\Gamma} \tag{4}$$

$$\text{and Auger yield}\quad a(f \rightarrow i) = \frac{\Gamma_{if}^A}{\Gamma}. \tag{5}$$

Here, the initial configuration is given by i decaying into the final configuration f. Γ is the sum of partial radiative widths Γ_{if}^R and non-radiative width Γ_{if}^A, given by

$$\Gamma = \sum_{i,f} \Gamma_{if}^R + \sum_{i,f} \Gamma_{if}^A. \tag{6}$$

The partial widths for radiative decay in a singly ionized atom are calculated (in atomic unit) as follows:

$$\Gamma_{if}^R(f \rightarrow i) = (4/3)(\Delta E/c)^3 \left|\langle \Psi_f \left| D \right| \Psi_i \rangle\right|^2 \tag{7}$$

where Ψ_i and Ψ_f are the initial and final states of the system, respectively. ΔE is the energy difference between these states, c is the speed of light. D is the electric dipole operator.

The non-radiative partial widths are obtained as:

$$\Gamma_{if}^A(f \rightarrow i) = \frac{2\pi}{\hbar} \bar{\sum} \left|\langle \Psi_f \left| H^{ee} \right| \Psi_i \rangle\right|^2 \rho(\varepsilon) \tag{8}$$

where H^{ee} is the operator of the electron-electron interaction. The density of final state $\rho(\varepsilon)$ is unity when the continuum-state wave function is normalized in the energy scale. The $\bar{\sum}$ denotes the average and the sum over the initial and the final states, respectively.

The calculations of radiative transition rates were performed for singly ionized atoms using Multiconfiguration Dirac Fock (MCDF) wave functions [22]. The non-radiative transition rates were computed with a code written by Lorenz and Hartmann [23] using Dirac Fock Slater (DFS) wave functions.

The electron shake-off process resulting from the sudden change of the atomic potential during vacancy cascade development, which can lead to the ejection of additional electrons through the atomic reorganization processes are calculated using the code written by El-Shemi [24]. In this way we calculate the electron shake-off probabilities according to Åberg [25,26] by overlapping integrals between the wave functions of initial state φ_i and the final state φ_f of the considered process. The probability of an electron transition from the orbital nlj to the orbital $n'l'j'$ is given by

$$p_{nlj \rightarrow n'l'j'} = \left| \int \varphi_{nlj}^*(\mathrm{A}_0) \varphi_{n'l'j'}(\mathrm{A}) d\tau \right|^2 \tag{9}$$

with $\varphi_{nlj}(\mathrm{A})$ and $\varphi_{n'l'j'}(\mathrm{A}_0)$ being orbital wave functions for the orbital nlj and for the orbital $n'l'j'$ in the ion A_0. Thereby the ion originates from the atom A by a change in the potential in the course of the ionization processes. The probability that at least one of the N electrons located in the subshell nlj becomes ionized is given by

$$p = 1 - \left(\left| \int \varphi^*_{nlj}(\mathrm{A}_0) \varphi_{n'l'j'}(\mathrm{A}) d\tau \right|^2 \right)^N - p_f \qquad (10)$$

where the quantity p_f represents a correction for physically not allowed transitions to occupied shells and has the form

$$p_f = \sum_{n'lj} N \frac{N'}{2j+1} \left| \int \varphi^*_{n'lj}(\mathrm{A}_0) \varphi_{nlj}(\mathrm{A}) d\tau \right|^2 \qquad (11)$$

with $n' \neq n$ and N' is the number of the electrons in the orbital $n'lj$.

The calculation technique is based on the simulation of the de-excitation vacancy cascade originating from a configuration with a single vacancy. Each cascade starts with the implementation of atomic data for all possible X-ray, Auger, Coster Kronig, and shake-off channels. To realize a Monte Carlo selection of the actual de-excitation channel, the probabilities of all de-excitation channels were normalized to 1. Then a random number generated in the interval [0,1] selected the next de-excitation step including vacancy transfer and ionization.

Let N denote the number of vacancies created in nl subshells of an atomic configuration via radiative or non-radiative transitions. For example, the configuration $1s\,2s^2\,2p^6\,3s^2\,3p^6$ would represent a distribution with a single K-shell vacancy ($N = 1$); $1s^2\,2s^2\,[2p^5]\,3s^2\,[3p^5]$ would represent a distribution that could be formed via a Coster Kronig transition. The electron symbol in the square brackets will be used to indicate spectator holes. After creating a new spectator vacancy in an actual configuration, the program first controls whether shake-off takes place or not. If the random number generated is smaller than the sum of all normalized shake-off probabilities of the preceding vacancy configuration, then a shake-off process takes place, i.e. an additional electron ejected in a higher subshell. The channel whose subshell shake-off probability value coincides with the random number generated will be activated. After the decision about the occurrence of a shake-off process the program selects the following de-excitation trees by generating a new random number. Here first a comparison of the value of the random number and the fluorescence yield proves whether radiative or non-radiative take place. The actual de-excitation channel after this decision is chosen in analogy with the determination of the shake-off channels. Each new configuration is analyzed to see if further decays are possible. If they are, then the program code goes back to the first step described above. The generation of new vacancy configurations continues until all vacancies have reached the outer shells or no further decays are possible. If no further decays are possible for any of the final configurations we have a complex de-excitation tree ending up with a great number of configurations each of which is characterized by its probability depending on its de-excitation history. The charge state degree of the ions with vacancies (Z_q) in the outer shells is recorded. After finishing the de-excitation tree the same inner shell vacancy will be simulated again. The probabilities of ion-charged state distributions $p(Z_q)$ and the average ion charge $\langle Z_q \rangle$ are recorded after 10^5 histories

$$p(Z_q) = \frac{\sum_1^{10^5} Z_q^i}{n} \qquad (12)$$

here the superscript i is denoted to the equal produced ionization degree for Z_q and n is the number of histories ($=10^5$) in our calculation. The mean charge state of ions is given by:

$$\langle Z_q \rangle = \sum p(Z_q^i) Z_q^i. \qquad (13)$$

The creation of multiple vacancies in atomic configurations during vacancy population causes transition energy shifts and may result in an energetic closing of channels for certain Coster-Kronig transitions. In the determination of the population of the multiple vacancy states, the vacancy cascade modeling takes into account the fact that the change of radiative and non-radiative transition rates occurs due to transition energy shifts. The correction of the transition rates quantum-mechanically requires more difficult calculations. Therefore the transition rates were calculated according to the following scheme. At first quantum mechanically determined transition rates were calculated for singly ionized atoms. The corrected transition rates for multi-ionized atoms having configurations with more vacancies are calculated using the scaling procedure proposed by Larkins [27]. So, the corrected radiative and non-radiative transition rates during vacancy cascade development are obtained using the following scaling procedure:

$$\text{for radiative} \quad \Gamma^r = n_1 \frac{(N_2 - n_2)}{N_2} \Gamma^R \qquad (14)$$

where n_1 and n_2 are the vacancies in initial and final states respectively. N_2 are the occupation numbers for the final state f. Γ^r are the radiative transition rates for multi-ionized atoms and Γ^R for singly ionized atoms

$$\Gamma^a = \frac{N_1 N_2}{(4l_1+2)(4l_2+2)} \Gamma^A \quad \text{for non-equivalent electrons} \qquad (15)$$

and

$$\Gamma^a = \frac{N_1(N_1-1)}{(4l_1+2)(4l_1+2-1)} \Gamma^A \quad \text{for equivalent electrons} \qquad (16)$$

where N_1 and N_2 are the occupation numbers for the final state f and l are the orbital quantum number. Γ^a are the non-radiative transition rates for multi-ionized atoms and Γ^A for singly ionized atoms.

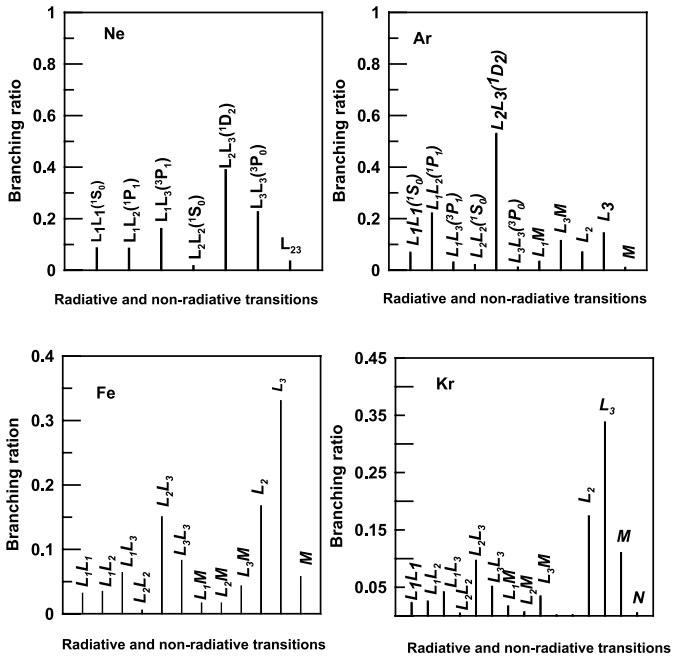

Fig. 1. Radiative and non-radiative branching ratios for the decay of Ne, Ar, Fe, and Kr atoms after K-shell ionization.

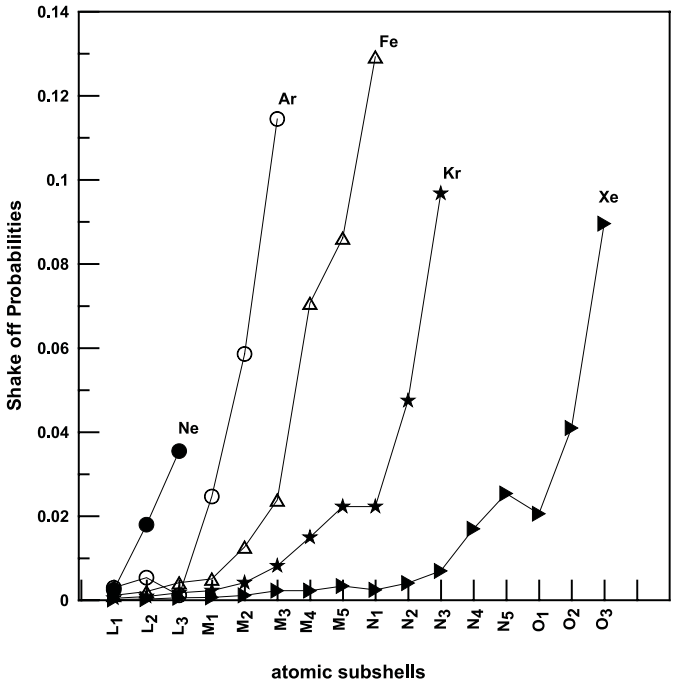

Fig. 2. Electron shake-off probabilities after K-shell ionization in Ne, Ar, Fe, Kr, and Xe atoms.

Because most Coster-Kronig energies are so low and the rates are so sensitive to the transition energy, some Coster-Kronig channels may be energetically forbidden during the cascade de-excitation decays. The production of various vacancies in intermediate configurations during the cascade decay is due to a closing of the Coster-Kronig channels. This effect will be considered in our treatment by using a semi-empirical approach, the so-called "$Z + 1$ rule" [28]. The Auger electron kinetic energy E_A is obtained from

$$E_{nl} - E_{n'l'} = E_{n''l''} + E_A \tag{17}$$

where E_{nl} and $E_{n'l'}$ are the binding energies for a neutral atom but $E_{n''l''}$ is the binding energy of an electron in $n''l''$ shell of the ion with a single positive charge due to a vacancy in $n'l'$ shell.

3 Results and discussions

The radiative and non-radiative branching ratios give valuable information on the de-excitation dynamic of an atom with a core vacancy. The branching ratios for possible radiative and non-radiative transitions from K-shell ionization in Ne, Ar, Fe, and Kr atoms are shown in Figure 1. The radiative transitions (X-ray transitions) are generally much weaker than non-radiative transitions for K-shell ionization in Ne. The dominant non-radiative channels are found to be K–L_2L_3 and K–L_3L_3 transitions. Consequently, the probability of filling the K-shell vacancy through Auger transitions is high. The decay of a K-shell vacancy in the Ne atom through non-radiative transitions leads to doubly charged ions. For Ar K-shell ionization, the K–L_2L_3 Auger channel is the strongest one. In Figure 1 it is shown that the radiative K–L transitions (X-ray transitions) are less than 20%, and the Auger electron emission is clearly the dominant mechanism for the production of the highly charged ions. The radiative transitions K–L are the dominant transitions for K-shell vacancy relaxation in Fe and Kr atoms. The K–L_3 ($K_{\alpha 1}$) transition is the strongest one after K-shell ionization in Fe and Kr atoms. This transition results from the fact that the inner-shell vacancies can be filled by successive Auger and Coster-Kronig transitions. These Auger and Coster-Kronig channels cause the emission of many Auger electrons and electron shake-off. Thereby, Coster-Kronig transitions are expected to play an important role in the formation of multiply charged ions following K-shell vacancy production in Fe and Kr atoms. The radiative and non-radiative branching ratios give valuable information on the de-excitation dynamic of an atom with a core vacancy.

Figure 2 shows the calculated results of electron shake-off probabilities caused by K-shell vacancy relaxation in Ne, Ar, Fe, Kr, and Xe atoms. It is found that the shake-off probabilities increase with increasing orbital quantum number (l) in atoms. The probability is higher in $2p_{3/2}$, $3p_{3/2}$, $3d_{5/2}$, $4p_{3/2}$ and $5p_{3/2}$ in Ne, Ar, Fe, Kr, and Xe, respectively. The importance of this process encourages us to consider it in the calculation of the charge state distributions formed in ionized atoms.

The charge state distribution of ions following de-excitation decay of vacancies after K-shell ionization in atoms from $Z = 10$ into $Z = 60$ are presented in Table 1. Results for $Z = 76$ and $Z = 80$ are added. The localization of a primary vacancy decisively determines the development of a vacancy cascade. Deeper vacancies lead to

Table 1. Ion charge state distributions (%) following de-excitation decay for different excited atoms with K-shell vacancy. Tabulated are contributions greater than 0.1%. q is final ion charge.

q	$Z=10$	$Z=12$	$Z=14$	$Z=16$	$Z=18$	$Z=19$	$Z=20$	$Z=22$	$Z=24$	$Z=25$	$Z=26$	$Z=30$
1	1.0			0.2	0.5	0.5						0.2
2	77.4	3.1	1.0	4.4	7.1	4.0	1.6	1.8	2.6	3.0	4.2	7.4
3	20.8	60.5	4.2	7.0	10.1	9.4	10.2	2.4	4.8	5.1	6.8	14.8
4	0.9	27.1	46.3	33.1	35.4	16.8	11.0	16.0	13.7	10.0	10.5	16.2
5		7.3	40.8	33.1	33.7	40.4	30.5	19.3	16.8	13.1	12.3	17.7
6		1.8	6.3	20.0	10.9	24.5	32.9	35.8	10.1	17.3	12.7	20.2
7		0.2	1.2	2.1	1.9	4.1	10.3	19.0	27.5	17.7	17.9	14.1
8			0.1	0.1	0.3	0.3	3.3	4.8	19.0	22.2	18.8	2.8
9							0.2	0.8	4.6	9.1	12.6	2.8
10								0.1	0.7	2.3	3.7	2.1
11											0.4	1.7
q	$Z=34$	$Z=36$	$Z=37$	$Z=38$	$Z=40$	$Z=44$	$Z=48$	$Z=50$	$Z=54$	$Z=60$	$Z=76$	$Z=80$
1	0.3	0.4	0.4	0.4	0.1	0.2	0.1	0.6	0.2	0.2	0.1	0.4
2	0.8	0.9	0.8	0.6	0.6	1.4	1.7	2.1	1.9	0.6	0.6	1.0
3	3.7	3.7	3.3	1.8	1.1	2.7	3.1	4.2	1.1	2.3	1.0	1.6
4	23.7	18.9	10.6	7.3	5.4	5.7	7.5	8.4	4.3	4.2	2.2	7.9
5	31.7	21.1	17.3	18.2	14.8	11.9	13.1	12.0	5.8	6.6	4.2	5.8
6	28.5	17.4	15.1	16.0	19.1	15.2	15.3	13.7	11.4	10.6	8.6	9.2
7	9.5	12.8	14.1	14.7	15.4	15.9	14.6	13.1	14.3	15.2	11.5	5.7
8	1.4	9.9	10.2	11.8	12.5	11.6	5.8	11.0	18.9	25.3	5.1	8.9
9	0.2	7.0	9.2	7.6	9.5	12.8	7.7	9.1	14.2	15.0	8.6	8.5
10		5.0	10.5	10.0	7.9	7.5	7.1	7.0	9.3	7.6	10.5	4.0
11		2.2	5.8	7.1	6.9	5.6	5.7	5.0	5.9	1.7	11.2	6.9
12		0.7	2.0	3.1	4.9	5.2	6.5	3.8	3.8	2.4	11.4	6.3
13		0.5	0.5	1.0	1.5	3.1	4.9	3.1	2.9	1.8	11.4	7.3
14		0.1	0.1	0.2	0.3	1.0	3.4	3.3	2.2	1.7	9.7	6.9
15						0.3	2.1	2.1	1.6	1.6	7.2	6.9
16							1.0	1.0	0.9	1.2	4.1	5.2
17							0.3	0.3	0.2	0.8	1.8	3.1
18										0.5	0.9	2.4
19										0.3	0.5	1.0
20										0.1	0.3	0.7
21											0.2	0.1

higher mean ion charge states and vacancies in outer shells produce only ions with some few additional vacancies because of the restricted number of possible de-excitation channels. For very complex atoms (e.g. $Z = 60$ to 80) it is less probable to find atoms with low charge states q after de-excitation processes.

The mean ion charge state $\langle Z_q \rangle$ is compared with available theoretical and experimental data in Table 2. The mean ion charge state after the de-excitation of inner-shell vacancies increases with increasing atomic number because of the increasing complexity of the atomic structure and the increasing number of possible non-radiative transitions.

Figure 3 shows the results of Ar^{q+} ions resulting from de-excitation decay after K-shell vacancy production in Ar atoms. The results are obtained by performing the calculation with and without considering the electron shake-off processes. The deviation in the results for charge state distributions with and without consideration of the electron shake-off probability demonstrates the importance of this process in the calculation of vacancy cascades in atoms. It is clear that the consideration of the electron shake-off process in the calculation of charge state distributions leads to good agreement with the experimental data. However, in Ar the present values of Ar^{7+} ions are slightly smaller than the experimental values. This is probably due to neglecting of double Auger effect in the present calculations. According to the experimental results of Carlson and Krause [6] the intensity of the double Auger process in Ar is about 10% relative to all non-radiative transitions.

Figure 4 shows the charge state distributions following de-excitation decay after K-shell vacancy production in Ne, Fe, Kr, and Xe atoms. The de-excitation of a primary K-shell vacancy in neon occurs with high probability by $1s^2$–$2s^22p^4$ Auger transitions because of the small K fluorescence yield ($\omega(\mathrm{Ne}) = 0.015$), the Auger yield is ($a = 0.985$). As a result of this KLL Auger

Table 2. The mean ion charge following K-shell vacancy de-excitation in atoms.

	$\langle Z_q \rangle$			
Z	Present work	Exp. [2]	Calc. [15]	Calc. [12]
10	2.2	2.2	1.9	2.0
12	3.4			
14	4.5			
16	4.6			
18	4.2	4.2	4.1	4.0
19	4.8			
20	5.3			
22	5.6			
24	6.1			
25	5.3			
26	6.3			
30	5.2			
34	5.2			
36	6.1	6.1	5.72	
38	7.1			
40	7.4			
44	7.6			
48	7.8			
50	7.6			
54	7.9	8.2		
60	8.6			
76	9.9			
80	10.1			

transitions the contribution of Ne^{2+} ions is 77.4%. New vacancies created by this process could not further decay by non-radiative electron transitions. The triple Ne^{3+} and quadratic Ne^{4+} ions are produced by electron shake-off processes exclusively. From this situation the production of vacancies in the outermost subshells occurs from shake-off processes, only if non-radiative de-excitation transitions are impossible.

The charge state distributions following K-shell vacancy de-excitation in Fe and other available theoretical values from the literature [16,17] are compared in Figure 4. The Fe 1s ionization mainly produces Fe^{6+}, Fe^{7+}, and Fe^{8+} ions, the doubly Fe^{2+} and triply Fe^{3+} charged ions appear weakly in the distribution. The spectrum of the number of ejected electrons after K-shell vacancy de-excitation forms an asymmetric peak. The probabilities of charge states are decreasing at lower and higher end of the distributions, and the most probable charge states appear in the middle of the distribution.

The calculated q value of Kr^{q+} ions produced following de-excitation of the primary K vacancy is compared with experimental and theoretical values in Figure 4. The ionization in the K-shell induces the multiply charged ions from Kr^{2+} to Kr^{13+}. The highest final charge state from K-shell hole is found to be Kr^{5+} ions. As shown from the figure, the present results agree well with experimental data.

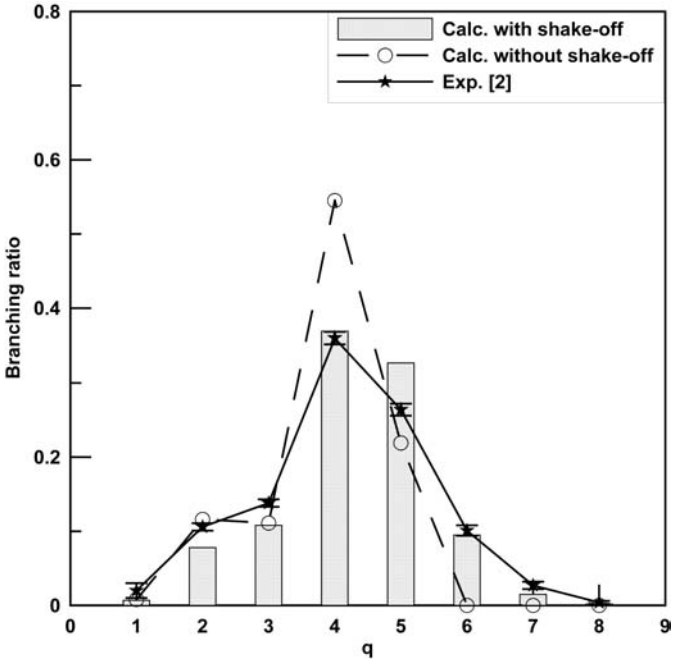

Fig. 3. The charge state distributions with and without consideration of shake-off processes in Ar atom after K-shell vacancy production.

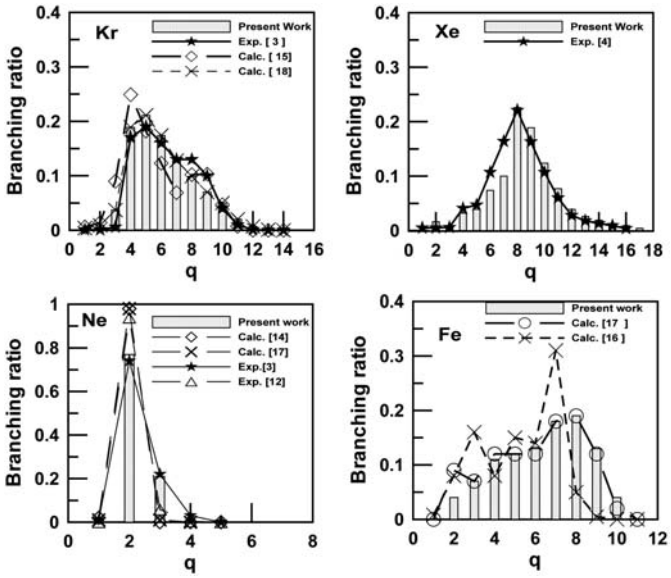

Fig. 4. The charge state distributions of ions after K-shell ionization in Ne, Fe, Kr, and Xe atoms.

Figure 4 shows the probability of final charge state distributions for Xe^{q+} ions after de-excitation of K vacancy. The calculation and experimental Xe^{q+} ion charge have a maximum at $q = 8$ and a shoulder at $q = 4$. It is connected with the initial K–$L_{2,3}$ radiative transitions which occur with (88.8%) probability replacing the vacancy to the $L_{2,3}$ subshells at the first decay step. Further non-radiative decays occur to fill the formed $L_{2,3}$ vacancies, which then decays through L–NN, L–NO and L–OO Auger transitions, lead to production of Xe^{4+} ions. Ions mainly

produced from Xe in K-shell vacancy state are found to be Xe^{7+}, Xe^{8+}, Xe^{9+}, and Xe^{10+}. The spectrum of the number of ejected electrons resulting from de-excitation decay of inner-shell vacancies in xenon forms a symmetric peak, e.g. the highest probable charge state with decreasing probabilities for charge states to the lower and higher end of the distribution. The results agree well with the available experimental data [4].

4 Conclusions

Ion charged state distributions and average number of ejected electrons following K-shell ionization in atoms are calculated using a Monte Carlo simulation technique. The radiative and non-radiative branching ratios for singly ionized atoms are obtained. The atomic data of radiative and non-radiative transitions for multi-ionized atoms are evaluated using a statistical scaling procedure based on the transition probabilities for singly ionized atoms. The electron shake-off processes resulting from the change of the atomic potential after inner-shell vacancy production are considered in the present work. The results of final charge state distributions agree well with the experimental data.

References

1. M.O. Krause, M.V. Vestal, W.H. Johnson, T.A. Carlson, Phys. Rev. **133**, A385 (1964)
2. T.A. Carlson, M.O. Krause, Phys. Rev. **137**, A1655 (1965)
3. M.O. Krause, T.A. Carlson, Phys. Rev. **158**, 18 (1967)
4. T.A. Carlson, W.E. Hunt, M.O. Krause, Phys. Rev. **151**, 41 (1966)
5. T.A. Carlson, M.O. Krause, Phys. Rev. **140**, A1054 (1965)
6. T.A. Carlson, M.O. Krause, Phys. Rev. Lett. **17**, 1079 (1966)
7. K. Ueda, E. Shigemasa, T. Sato, A. Yagishita, M. Ukai, H. Maezawa, T. Hayaishi, T. Sasaki, J. Phys. B: At. Mol. Opt. Phys. **24**, 605 (1991)
8. T. Hayaishi, Y. Morioka, Y. Kageyama, M. Watanabe, I.H. Suzuki, A. Mikuni, G. Isoyama, S. Asaoka, M. Nakamura, J. Phys. B: At. Mol. Phys. **20**, L287 (1987)
9. T. Mukoyama, T. Tonuma, A. Yagishita, H. Shibata, T. Matsuo, K. Shima, H. Tawara, J. Phys. B: At. Mol. Phys. **20**, 4453 (1987)
10. N. Saito, I.H. Suzuki, J. Phys. B: At. Mol. Opt. Phys. **25**, 1785 (1992)
11. H. Tawara, T. Hayaishi, T. Koizumi, T. Matsuo, K. Shima, A. Yagishita, J. Phys. B: At. Mol. Opt. Phys. **25**, 1476 (1992)
12. G. Omar, Y. Hahn, Phys. Rev. A **43**, 4695 (1991)
13. G. Omar, Y. Hahn, Phys. Rev. A **44**, 483 (1991)
14. A.G. Kochur, A.I. Dudenko, V.L. Sukhorukov, I.D. Petrov, J. Phys. B: At. Mol. Opt. **27**, 1709 (1994)
15. A.G. Kochur, A.I. Dudenko, V.L. Sukhorukov, I.D. Petrov, J. Phys. B: At. Mol. Opt. **28**, 387 (1995)
16. V.L. Jacobs, J. Davis, F.B.F. Rozsnyai, J.W. Cooper, Phys. Rev. A **21**, 1917 (1980)
17. M.G. Opendak, Astrophys. Space Sci. **165**, 9 (1990)
18. T. Mukoyama, Bull. Inst. Chem. Res. Kyoto Univ. **63**, 373 (1985)
19. N. Mirakhmedov, E.S. Parilis, J. Phys. B: At. Mol. Opt. Phys. **21**, 795 (1988)
20. A.M. El-Shemi, A.A. Ghoneim, Y.A. Lotfy, Turk. J. Phys. **27**, 51 (2003)
21. A.H. Abdullah, A.M. El-Shemi, A.A. Ghoneim, Rad. Phys. Chem. **68**, 697 (2003)
22. I.P. Grant, B.J. Mckenzie, P. Norrington, D.F. Mayers, N.C. Pyper, Comput. Phys. Commun. **21**, 207 (1980)
23. M. Lorenz, E. Hartmann, Report ZFI-109, Leipzig **27** (1985)
24. A. El-Shemi, Egypt. J. Phys. **27**, 231 (1996)
25. T. Åberg, Phys. Rev. **156**, 35 (1967)
26. T. Åberg, Ann. Acad. Sci. Finn. Ser. AVI Phys. **308**, 7 (1969)
27. F.P. Larkins, J. Phys. B: At. Mol. Phys. **4**, L29 (1971)
28. M.F. Chung, L.H. Jenkins, Surf. Sci. **22**, 479 (1970)